

Efficient Acceleration of High-Quality GeV-Electron Bunches in a Hybrid Laser- and Beam-Driven Plasma Wakefield Accelerator

F. M. Foerster,^{1,*} M. Ayache,¹ Z. Bi,¹ M. Cerchez,² S. Corde,³ A. Döpp,^{1,4} F. Haberstroh,¹ A. F. Habib,⁵ T. Heinemann,² B. Hidding,² A. Irman,⁶ F. Irshad,¹ O. Kononenko,³ M. LaBerge,⁶ A. Martinez de la Ossa,⁷ A. Münzer,¹ F. Peña,^{1,8} G. Schilling,¹ S. Schöbel,^{6,9} U. Schramm,^{6,9} S. Sharan,¹ E. Travac,¹ P. Ufer,^{6,9} N. Weiße,¹ M. Zeuner,¹ J. Zirkelbach,¹ and S. Karsch^{1,4,†}

¹Ludwig-Maximilians-Universität München, Am Coulombwall 1, 85748 Garching, Germany

²Heinrich Heine Universität Düsseldorf, Universitätsstraße 1, 40225 Düsseldorf, Germany

³Laboratoire d'Optique Appliquée (LOA), CNRS, École polytechnique, ENSTA, Institut Polytechnique de Paris, Palaiseau, France

⁴Max Planck Institut für Quantenoptik, Hans-Kopfermann-Strasse 1, 85748 Garching, Germany

⁵University of Strathclyde, 107 Rottenrow, Glasgow G4 0NG, United Kingdom

⁶Helmholtz-Zentrum Dresden-Rossendorf, Bautzner Landstrasse 400, 01328 Dresden, Germany

⁷Deutsches Elektronen-Synchrotron DESY, Notkestraße 85, 22607 Hamburg, Germany

⁸Department of Physics, University of Oslo, 0316, Oslo, Norway

⁹Technische Universität Dresden, 01062 Dresden, Germany

(Dated: March 2, 2026)

Plasma-based accelerators are compact and provide high gradients, yet their practical use has been limited by energy gain, stability, beam quality, and energy transfer efficiency. Here, we address several of these challenges simultaneously using a hybrid scheme in which an electron bunch from a laser wakefield accelerator (LWFA) drives a subsequent plasma wakefield accelerator (PWFA) stage with internal witness injection. Close to driver depletion in the PWFA stage, we obtain witness bunches with higher electron energy, reduced energy spread and divergence, and higher angular-spectral charge density compared to LWFA alone. We report energy transformer ratios approaching 2, and about 20% of the initial energy in the drive beam was transferred to the witness bunch, thereby achieving a driver-to-witness energy transfer efficiency that largely surpasses that of all previous PWFA experiments.

Introduction.—The demand for more compact and cost-effective particle accelerators has spurred the exploration of novel acceleration concepts beyond conventional radio-frequency (rf) technologies. Among these, plasma-based accelerators have emerged as a promising candidate due to their ability to sustain accelerating gradients several orders of magnitude higher than those in rf-accelerating structures [1–3]. Laser- and beam-driven plasma wakefield accelerators (LWFAs and PWFAs) have demonstrated significant progress in recent years, providing electron bunches with ultrashort duration [4–6] and high peak currents [7–9]. Over the years, plasma accelerators have seen steady improvements in energy gain [10–14], spectral quality [15, 16], stability [17], and energy transfer efficiency [7, 18]. However, optimizing multiple beam parameters simultaneously remains a major challenge, as trade-offs between these often limit performance in practical scenarios. Application-oriented beams demand a careful balance between these objectives, motivating new approaches that can break current limitations.

A promising path forward is offered by the hybrid laser- and beam-driven plasma wakefield accelerator (LWFA-PWFA), which aims to combine the complementary strengths of LWFA and PWFA stages [7, 17, 19–24]. LWFAs benefit from the wide availability of high-power laser systems. However, their operation is challenged by the combined effects of dephasing between the elec-

trons and the driving laser pulse, laser diffraction, and plasma-electron heating from the laser's oscillatory field. Although each of these issues can be mitigated individually, their simultaneous presence makes it difficult to achieve high-energy and ultralow-emittance electron bunches. Moreover, the properties of electron bunches obtained from LWFA are particularly susceptible to shot-to-shot fluctuations in the laser output and its subsequent nonlinear propagation in the plasma [25, 26]. In contrast, PWFAs using ultrarelativistic charged particle beams as drivers are dephasingless and, when combined with suitable injection schemes, could produce witness bunches with exceptionally low transverse emittance [27, 28]. Their main limitation lies in the scarcity of suitable drive bunches, which typically require access to large-scale accelerator facilities [29–32]. By leveraging an LWFA-generated electron bunch to drive a subsequent PWFA stage, the hybrid approach offers a practical route to harness the advantages of both plasma accelerator concepts within a compact setup.

The hybrid LWFA-PWFA concept evolved from the observation of collective deceleration of LWFA-generated electrons in a plasma [20, 21], to a dedicated two-stage configuration, although with limited control over witness injection in the PWFA stage [22], and eventually to controlled internal down ramp injection of witness bunches in the PWFA stage [23]. More recently, we have begun

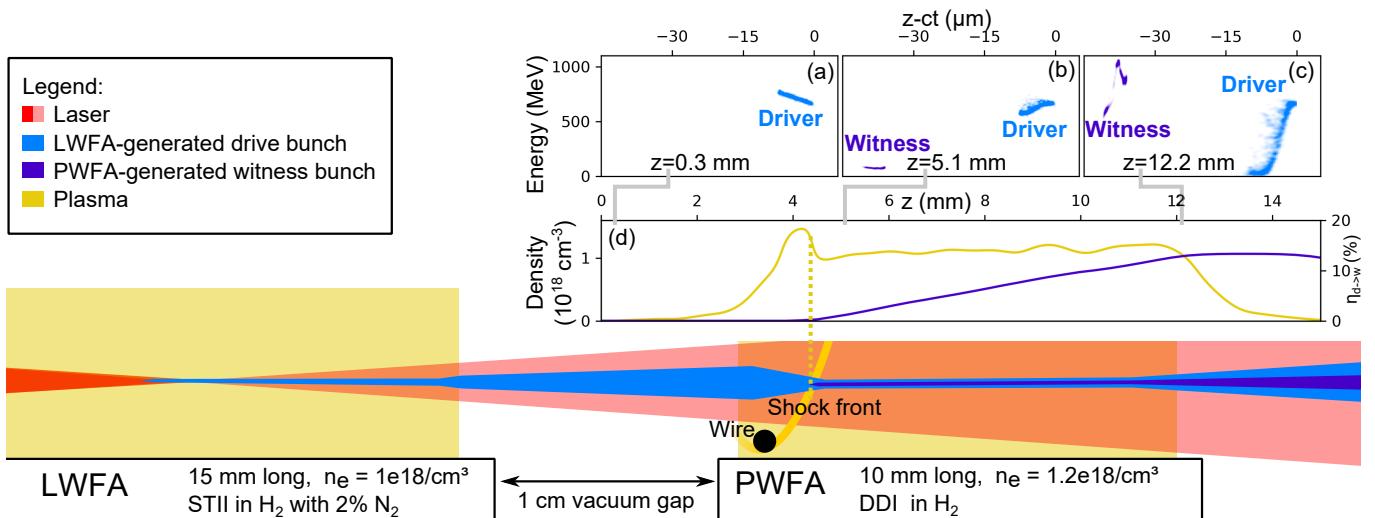


FIG. 1. Schematic setup for the experimental generation of high-energy, high-quality witness bunches in a hybrid LWFA-PWFA. In the LWFA stage, electron bunches are generated via self-truncated ionization injection (STII). After a vacuum gap, these electron bunches (light blue) drive the PWFA stage. A wire-generated shock (orange) enables the density down ramp injection (DDI) of witness electrons (violet) into the PWFA stage. Insets (a)–(c) show the longitudinal phase space of driver and witness retrieved from an exemplary PIC simulation at different positions in the PWFA stage [33]. (d) shows the plasma density distribution of the PWFA together with the evolution of the driver-to-witness energy transfer efficiency along the length of the PWFA stage.

leveraging the full potential of this configuration, demonstrating high stability and an enhanced angular-spectral charge density of the witness bunch compared with the initial LWFA-generated drive bunch [17]. While these experiments have revealed the potential of hybrid LWFA-PWFA as a beam quality booster [34], a booster for the peak electron energy [35] has not yet been experimentally verified. In all previous experiments, the peak electron energy of the witness bunch has remained limited to values lower than that of the driver, and the driver-to-witness energy transfer efficiency of the PWFA stage has not yet been fully exploited.

In this work, we present witness bunches from a hybrid LWFA-PWFA setup, characterized by higher electron energy, lower energy spread, and lower divergence than the LWFA-generated drive bunches. At the same time, the driver-to-witness energy transfer efficiency reaches unprecedentedly high values of $\sim 20\%$. Furthermore, we conduct a careful review of various measures used in the literature to characterize the electron energy gain and efficiency of plasma-based accelerators. Based on this, we compare our results to the current state of the art.

Experimental setup.—The experiments were performed at the Centre for Advanced Laser Applications in Garching, Germany. The hybrid LWFA-PWFA setup consists of two consecutive gas targets separated by a 1 cm vacuum gap (see Fig. 1). The first stage is an LWFA, driven by a Ti:sapphire laser pulse with ≈ 9 J on-target energy, 30 fs (FWHM) pulse duration at a central wavelength of 800 nm. The laser pulse is focused with an $f/47$ geometry to a peak intensity of $(1.6 \pm 0.3) \times 10^{19}$ W/cm²,

which corresponds to a normalized vector potential of $a_0 \approx 2.7$. The target is a 15 mm-long slit nozzle operated with hydrogen gas doped with 2% nitrogen gas at a plasma density of 1.0×10^{18} cm⁻³. Electron injection in the LWFA occurs via self-truncated ionization injection [8, 36–38], which relies on rapid laser self-focusing in a low-ionization-threshold background gas, followed by ionization of inner-shell electrons from the dopant species. This configuration produces electron bunches with charge of 366 ± 69 pC (mean and standard deviation of the integrated charge above 200 MeV), a rms-divergence of 0.9 ± 0.1 mrad (mean and standard deviation from gaussian fit), a peak electron energy of 716 ± 44 MeV (mean and standard deviation), and a relative FWHM-energy spread of $9\% \pm 3\%$ (mean and standard deviation) as measured using an absolutely calibrated dipole spectrometer.

The subsequent PWFA stage employs the LWFA-generated electron bunch as the driver. The beam axis was positioned close (2 mm) above the exit face of the 10 mm-long supersonic slit nozzle to minimize density ramps at both ends (see Fig. 1(d)). The remaining laser from the LWFA stage ionizes the gas homogeneously in a ~ 1 mm wide column around the optical axis. However, it is no longer intense enough to excite a wakefield itself in the second target after diffracting in the 1-cm vacuum gap between the stages [17]. The PWFA stage is operated with pure hydrogen gas at a plasma density of 1.2×10^{18} cm⁻³. Controlled injection of a witness beam is achieved via a hydrodynamic shock, generated by placing a thin wire in the supersonic gas flow. The resulting lo-

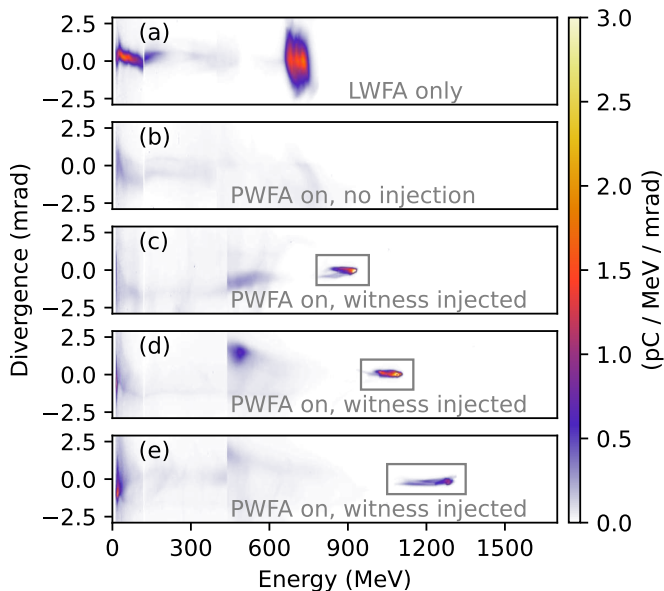


FIG. 2. Energy spectra of electron driver and witness for various conditions of hybrid LWFA-PWFA. (a) LWFA-generated drive beam. (b) Decelerated drive beam after the PWFA stage, without internal injection. (c) Decelerated driver and a typical internally injected witness after the PWFA stage. (d) Witness with the highest driver-to-witness energy transfer efficiency. (e) Witness with highest peak electron energy. Gray boxes highlight the spectral feature recognized as the witness. See [33] for detailed beam parameters.

calized density transition provides conditions suitable for density down ramp injection into the wakefield [17, 23].

Experimental results.—Figure 2(a) shows the measured energy spectrum of an exemplary electron bunch generated by the LWFA stage. When the PWFA target is activated without the hydrodynamic shock (i.e., without the injection mechanism), the drive beam is collectively decelerated in a self-driven plasma wave, leaving behind a low-charge continuous energy spectrum (see Fig. 2(b)). Upon insertion of the wire into the supersonic gas flow, thereby introducing a shock-induced density transition, witness electrons are injected and subsequently accelerated. The three representative witness bunches in Figure 2(c)-(e) have charges between 38 – 53 pC (integrated over full bunch), a divergence at the spectral peak energy of ~ 0.1 mrad (rms of gaussian fit), and energy spreads of 3-7% (FWHM).

We control the injection point within the plasma by varying the wire’s axial position, thereby adjusting the effective acceleration length. Figure 3(a) shows the injection positions relative to the measured (unperturbed) plasma density profile. For the longest acceleration length, we consistently obtain witness electron energies higher than the drivers’. The highest measured electron energy gain is around 1.3 GeV or about 1.8 times the driver peak electron energy. To our knowledge, this is among the highest witness electron energy gains (rela-

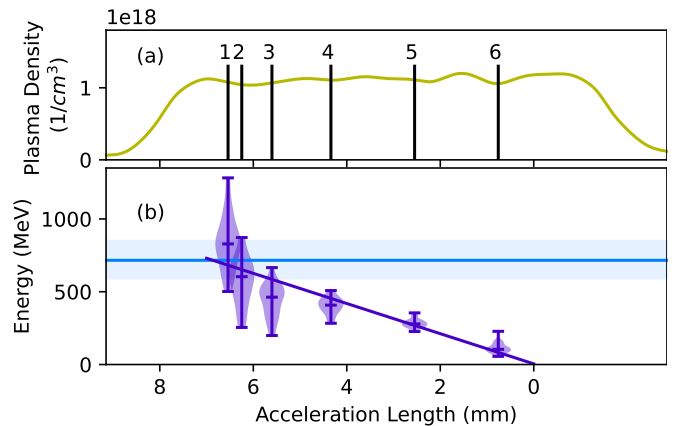


FIG. 3. Tuning the witness energy by variation of the injection position. (a) Interferometric measurement of the unperturbed plasma density distribution and definition of injection positions. (b) Mean peak witness electron energies and their distribution as a function of acceleration length (violet). The zero position of the x-axis is chosen to coincide with the zero-crossing of the linear fit and corresponds to a position close to the end of the PWFA plasma target. For comparison, the drivers’ mean peak electron energy and its min/max deviation are plotted in light blue.

tive to the driver electron energy) in all previous PWFA experiments and has only recently been surpassed [14] (see also Fig. 4 and the supplemental material [33]).

We record the peak energy of the accelerated witness beam as a function of the remaining acceleration length. Assuming a non-evolving strength of the wakefield, we use a linear fit to these data to estimate the average accelerating gradient in the PWFA stage of 104 GV/m, as shown in Figure 3(b). For late injection positions that result in moderate witness energies, we observe increased energy stability. For example, at injection positions 4 and 5, the peak energy fluctuates by $\sim 10\%$ only, consistent with the findings of our previous publication [17].

To interpret the maximum energy gain of a witness bunch in a beam-driven plasma accelerator, we first consider the two main limiting factors: (1) The accelerating gradient on the witness beam, and (2) the depletion of the driver, i.e. the point at which (a part of) the drive beam has lost all its kinetic energy to the plasma.

The transformer ratio of the wakefield relates the driver’s deceleration to the witness’s acceleration. Different definitions of the transformer ratio are used in the literature. The voltage transformer ratio is defined as the absolute value of the ratio of the peak accelerating field experienced by the witness beam to the peak decelerating field acting on the driver [39]. While the voltage transformer ratio is directly accessible in particle-in-cell (PIC) simulations, it is not easily measurable in experiments. As an experimentally accessible quantity, one can define an energy transformer ratio as the ratio of the final peak electron energy of the witness bunch to the maximum

electron energy loss of the drive bunch. This definition effectively captures the average voltage transformer ratio over the entire acceleration length. Note that under our experimental conditions, we can replace the electron energy loss of the driver with its peak electron energy before PWFA, because we completely decelerate (parts of) the drive bunch. Furthermore, since we inject our witness internally, and it therefore starts at zero energy, the energy transformer ratio is identical to the relative electron energy gain of the witness introduced above.

The PIC simulation in Fig 1(a)-(c) visualizes the evolution of the longitudinal phase space of the driver and witness through the PWFA stage and illustrates factors that limit the achievable energy transformer ratio. Any energy loss of the driver prior to witness injection, such as that occurring in a long density upramp of the plasma target, reduces the energy transformer ratio. Also, a non-optimal witness phase position reduces the energy transformer ratio. It can arise from plasma density variations, or from the onset of driver depletion [24, 40], causing parts of the drive beam to fall back in phase and distort the wakefield structure.

To boost the energy transformer ratios beyond previously reported values, we incorporated these considerations into the design of the plasma target. We choose the plasma length to terminate the acceleration close to the point of beam breakup due to the depletion of parts of the drive bunch, as seen in Fig. 1(c). Furthermore, as can be seen comparing Figure 1(a) and (b), the driver loses only a small part of its energy in the short density up-ramp. At the same time, this section is long enough for the drive bunch to self-focus after the vacuum drift section and to drive a strong wakefield at the point of injection.

Beyond a high energy transformer ratio, our PWFA stage is characterized by an unprecedentedly high energy transfer efficiency. As for the transformer ratio, different definitions of energy transfer efficiency are used in the literature, describing different aspects of energy transfer between driver, plasma, and witness bunch [15, 41, 42]. A first definition divides the integrated energy gain of the witness bunch $\Delta\varepsilon_W$ by the integrated energy of the incident drive bunch ε_D and corresponds to the driver-to-witness energy transfer efficiency: $\eta_{D \rightarrow W} = \frac{\Delta\varepsilon_W}{\varepsilon_D}$.

In a second definition, $\Delta\varepsilon_W$ is divided by the integrated energy loss of the driver $\Delta\varepsilon_D$. Assuming that all energy lost by the driver ended up in the plasma, this can be identified as the plasma-to-witness energy transfer efficiency: $\eta_{P \rightarrow W} = \frac{\Delta\varepsilon_W}{\Delta\varepsilon_D}$, where the integrated beam energy of driver and witness is $\varepsilon_{D/W} = \int \rho_Q(E) E dE$, and ρ_Q is the spectral charge density of driver and witness, respectively. $\Delta\varepsilon_{D/W}$ is the difference in integrated energy before and after the PWFA stage.

While both metrics for efficiency capture complementary aspects of energy coupling, they may differ significantly in magnitude. Caution is therefore required

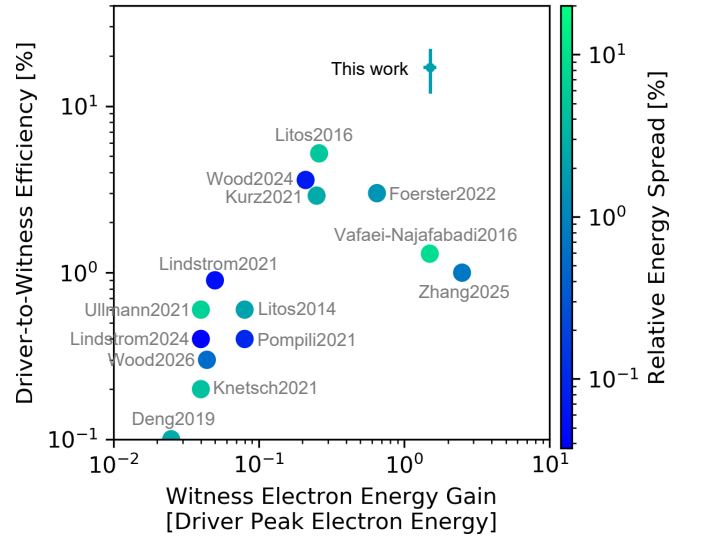


FIG. 4. Comparison of published PWFA results in terms of electron energy gain of the witness normalized to the peak electron energy of the respective driver, driver-to-witness energy transfer efficiency, and relative energy spread of the witness. The error bars for this work correspond to the uncertainties discussed in the supplemental material [33]. Note the logarithmic scale of all three categories.

when comparing efficiencies across different experiments or publications.

We analyze the energy transfer efficiencies for the high-quality witness bunches with a final electron energy exceeding the driver electron energy, as clear spectral separation is ensured. The shot with the highest measured energy transfer efficiency is shown in Figure 2(d). Its integrated energy is $\Delta\varepsilon_{\text{witness}} = 66$ mJ, and that of the drive bunch is $\varepsilon_{\text{driver}} = (274 \pm 61)$ mJ (run average and standard deviation). As we can not measure charge and energy of drive bunches before and after the PWFA stage individually, the exact integrated driver energy on the selected shot is unknown. Instead, we calculate a lower limit for the peak driver-to-witness energy transfer efficiency by assuming the integrated driver energy equals the highest value measured among all analyzed LWFA shots. This yields an efficiency:

$$\eta_{D \rightarrow W} \geq \frac{66 \text{ mJ}}{384 \text{ mJ}} = 17\%.$$

Using the average integrated driver energy instead, this value increases to 24%. Averaging over all shots with witness peak energies larger than 700 MeV, we find $\eta_{D \rightarrow W} = (7 \pm 5)\%$ (mean and standard deviation). For a discussion of systematic uncertainties and the large shot-to-shot variations of these numbers, see [33].

A value of $\eta_{D \rightarrow W} \geq 17\%$ is the highest driver-to-witness energy transfer efficiency observed in PWFA to date. Comparing the efficiencies $\eta_{D \rightarrow W}$ visualized in Figure 4, the results of this work outperform previous ex-

periments with either external [15, 18, 22, 32, 43, 44] or internal [17, 45–48] injection, by far [33].

Regarding plasma-to-witness energy transfer, we calculate a lower bound using the measured average energy remaining in the driver bunch after PWFA (~ 100 mJ) and by assuming that the spent driver energy actually contributed to driving the wakefield. At our experimental working point, we find

$$\eta_{P \rightarrow W} \geq \frac{66 \text{ mJ}}{(274 - 104) \text{ mJ}} = 39\%.$$

Similar values of $\eta_{P \rightarrow W}$ have only been reported from experiments operated far from driver depletion [15, 43, 44], where the peak electron energy of the witness changes by a small fraction of the driver’s peak electron energy only. Thus, while achieving very high plasma-to-witness energy transfer efficiency at their respective working points, a significantly lower fraction of the integrated drive beam energy is extracted in these previous experiments, resulting in a substantially lower driver-to-witness energy transfer efficiency.

Conclusion and Outlook.—In summary, we have demonstrated a hybrid LWFA-PWFA operated close to driver depletion and with internal witness injection. This experiment achieves high beam quality, a high energy transformer ratio close to two, record witness energies for this scheme of 1.3 GeV, and unprecedented driver-to-witness energy transfer efficiency of $\sim 20\%$, by far exceeding those of any previous PWFA experiment.

These experimental results on energy transfer efficiency and energy transformer ratio represent a long-sought breakthrough. While a high degree of driver depletion [41, 42] and a high plasma-to-witness energy transfer efficiency [15] have already been demonstrated individually, this is the first experiment to show both simultaneously, thus enabling the high driver-to-witness energy transfer efficiency. The measured energy transformer ratio is already within the range of theoretically predicted values for the voltage transformer ratio using symmetric bunches [39]. Further improvement can be expected by shaping the drive current [49–51]. In experiments to date, however, very high voltage transformer ratios have been shown only in regimes with low witness electron energy gain [52, 53].

In Figure 4, we compare published PWFA results in terms of electron energy gain of the witness normalized to the peak electron energy of the respective driver, and their driver-to-witness energy transfer efficiency. This comparison reveals a correlation between the two properties, led and confirmed by our experimental results.

Notably, our hybrid LWFA-PWFA scheme is not only at the forefront of driver-to-witness energy transfer efficiency but also generates dense, low-divergence (~ 0.1 mrad), and narrow-energy-spread (few %, compare color bar in Fig. 4) electron bunches. In terms of their low divergence and high charge density, our results

are on par with, or even better than, those in a similar energy regime achieved with LWFA alone [16], enabling the practical application of plasma-based accelerators. Recently, several groups have shown laser-like emission and the onset of exponential gain in free-electron lasers (FEL) driven by LWFA-generated beams [54–56]. Hybrid LWFA-PWFA could be considered as a compact and cost-efficient add-on for LWFA experiments, as FELs could particularly benefit from the improvements in beam parameters demonstrated here [57, 58]. Future research on these FEL applications should address full phase space measurements, including bunch current and emittance [4, 6, 59].

A further application of the high-energy, high-charge-density electron bunches with low divergence could be to explore strong-field quantum electrodynamics, e.g., in the non-perturbative Breit–Wheeler pair-production regime [60]. Here, increasing electron energy is essential to achieve large quantum nonlinearity parameters, while higher charge density and lower divergence enhance event rates in these intrinsically rare processes. Looking further into the future, the hybrid LWFA-PWFA can also serve as a versatile miniature test bed for studying the physics of next-generation plasma-based high-energy accelerators [61], replicating all key physical processes, and being experimentally accessible and operational today.

Acknowledgments.—We thank the Federal Republic of Germany and the Free State of Bavaria for funding the CALA infrastructure (15171 E 0002) and its operation. This work was supported by BMBF projects FIMO, MACLIP, and HyBright. F.M.F. is part of the Max Planck School of Photonics, supported by BMBF, Max Planck Society, and Fraunhofer Society. B.H., T.H., M.C., and F.A.H. are supported by the European Research Council (ERC) under the EU Horizon 2020 research and innovation programme (NeXsource: Next-generation Plasma-based Electron Beam Sources for High-brightness Photon Science, ERC Grant agreement No. 865877).

* moritz.foerster@physik.uni-muenchen.de

† stefan.karsch@physik.uni-muenchen.de

- [1] T. Tajima and J. M. Dawson, *Physical Review Letters* **43**, 267 (1979).
- [2] E. Esarey, C. B. Schroeder, and W. P. Leemans, *Reviews of Modern Physics* **81**, 1229 (2009).
- [3] C. A. Lindström, S. Corde, R. D’Arcy, S. Gessner, M. Gilljohann, M. J. Hogan, and J. Osterhoff, *Beam-driven plasma-wakefield acceleration* (2025), 2504.05558 [physics].
- [4] M. Heigoldt, A. Popp, K. Khrennikov, J. Wenz, S. W. Chou, S. Karsch, S. I. Bajlekov, S. M. Hooker, and B. Schmidt, *Physical Review Special Topics-Accelerators and Beams* **18**, 121302 (2015).
- [5] O. Zarini, J. C. Cabadağ, Y.-Y. Chang, A. Köhler,

- T. Kurz, S. Schöbel, W. Seidel, M. Bussmann, U. Schramm, A. Irman, and A. Debus, *Physical Review Accelerators and Beams* **25**, 012801 (2022).
- [6] M. LaBerge, B. Bowers, Y.-Y. Chang, J. Couperus Cabadağ, A. Debus, A. Hannasch, R. Pausch, S. Schöbel, J. Tiebel, P. Ufer, A. Willmann, O. Zarini, R. Zgadzaj, A. H. Lumpkin, U. Schramm, A. Irman, and M. C. Downer, *Nature Photonics*, 1 (2024).
- [7] J. Götzfried, A. Döpp, M. F. Gilljohann, F. M. Foerster, H. Ding, S. Schindler, G. Schilling, A. Buck, L. Veisz, and S. Karsch, *Physical Review X* **10**, 041015 (2020).
- [8] J. P. Couperus, R. Pausch, A. Köhler, O. Zarini, J. M. Krämer, M. Garten, A. Huebl, R. Gebhardt, U. Helbig, S. Bock, K. Zeil, A. Debus, M. Bussmann, U. Schramm, and A. Irman, *Nature Communications* **8**, 1 (2017).
- [9] C. Emma, N. Majernik, K. K. Swanson, R. Ariniello, S. Gessner, R. Hessami, M. J. Hogan, A. Knetsch, K. A. Larsen, A. Marinelli, B. O'Shea, S. Perez, I. Rajkovic, R. Robles, D. Storey, and G. Yocky, *Physical Review Letters* **134**, 085001 (2025).
- [10] I. Blumenfeld, C. E. Clayton, F. J. Decker, M. J. Hogan, C. K. Huang, R. Ischebeck, R. Iverson, C. Joshi, T. Katsouleas, N. Kirby, W. Lu, K. A. Marsh, W. B. Mori, P. Muggli, E. Oz, R. H. Siemann, D. Walz, and M. M. Zhou, *Nature* **445**, 741 (2007).
- [11] A. J. Gonsalves, K. Nakamura, J. Daniels, C. Benedetti, C. Pieronek, T. C. H. de Raadt, S. Steinke, J. H. Bin, S. S. Bulanov, J. van Tilborg, C. G. R. Geddes, C. B. Schroeder, C. Toth, E. Esarey, K. Swanson, L. Fan-Chiang, G. Bagdasarov, N. Bobrova, V. Gasilov, G. Korn, P. Satorov, and W. P. Leemans, *Physical Review Letters* **122**, 084801 (2019).
- [12] A. Picksley, J. Stackhouse, C. Benedetti, K. Nakamura, H. E. Tsai, R. Li, B. Miao, J. E. Shrock, E. Rockafellow, H. M. Milchberg, C. B. Schroeder, J. van Tilborg, E. Esarey, C. G. R. Geddes, and A. J. Gonsalves, *Physical Review Letters* **133**, 255001 (2024).
- [13] J. E. Shrock, E. Rockafellow, B. Miao, M. Le, R. C. Hollinger, S. Wang, A. J. Gonsalves, A. Picksley, J. J. Rocca, and H. M. Milchberg, *Physical Review Letters* **133**, 045002 (2024).
- [14] C. Zhang, D. Storey, A. Knetsch, B. D. O'Shea, R. Ariniello, G. J. Cao, S. Corde, T. N. Dalichaouch, C. Emma, O. G. Finnerud, S. Gessner, C. Hansel, E. Hansen, V. Lee, C. A. Lindstrøm, M. Litos, N. Majernik, K. A. Marsh, W. B. Mori, I. Rajkovic, M. J. Hogan, and C. Joshi, *Nature Communications* **16**, 10719 (2025).
- [15] C. A. Lindstrøm, J. M. Garland, S. Schröder, L. Boulton, G. Boyle, J. Chappell, R. D'Arcy, P. Gonzalez, A. Knetsch, V. Libov, G. Loisch, A. Martinez de la Ossa, P. Niknejadi, K. Pöder, L. Schaper, B. Schmidt, B. Sheeran, S. Wesch, J. Wood, and J. Osterhoff, *Phys. Rev. Lett.* **126**, 014801 (2021).
- [16] L. T. Ke, K. Feng, W. T. Wang, Z. Y. Qin, C. H. Yu, Y. Wu, Y. Chen, R. Qi, Z. J. Zhang, Y. Xu, X. J. Yang, Y. X. Leng, J. S. Liu, R. X. Li, and Z. Z. Xu, *Physical Review Letters* **126**, 214801 (2021).
- [17] F. M. Foerster, A. Döpp, F. Haberstroh, K. v. Grafenstein, D. Campbell, Y.-Y. Chang, S. Corde, J. P. Couperus Cabadağ, A. Debus, M. F. Gilljohann, A. F. Habib, T. Heinemann, B. Hidding, A. Irman, F. Irshad, A. Knetsch, O. Kononenko, A. Martinez de la Ossa, A. Nutter, R. Pausch, G. Schilling, A. Schletter, S. Schöbel, U. Schramm, E. Travac, P. Ufer, and S. Karsch, *Physical Review X* **12**, 041016 (2022).
- [18] M. Litos, E. Adli, J. M. Allen, W. An, C. I. Clarke, S. Corde, C. E. Clayton, J. Frederico, S. J. Gessner, S. Z. Green, M. J. Hogan, C. Joshi, W. Lu, K. A. Marsh, W. B. Mori, M. Schmeltz, N. Vafaei-Najafabadi, and V. Yakimenko, *Plasma Physics and Controlled Fusion* **58**, 034017 (2016).
- [19] B. Hidding, R. Assmann, M. Bussmann, D. Campbell, Y.-Y. Chang, S. Corde, J. C. Cabadağ, A. Debus, A. Döpp, M. Gilljohann, J. Götzfried, F. M. Foerster, F. F. Haberstroh, F. Habib, T. Heinemann, D. Holatz, A. Irman, M. Kaluza, S. Karsch, O. Kononenko, A. Knetsch, T. Kurz, S. Kuschel, A. Köhler, A. M. de la Ossa, A. Nutter, R. Pausch, G. Raj, U. Schramm, S. Schöbel, A. Seidel, K. Steiniger, P. Ufer, M. Yeung, O. Zarini, and M. Zepf, *Photonics* **10**, 99 (2023).
- [20] S. Chou, J. Xu, K. Khrennikov, D. E. Cardenas, J. Wenz, M. Heigoldt, L. Hofmann, L. Veisz, and S. Karsch, *Physical Review Letters* **117**, 144801 (2016).
- [21] M. F. Gilljohann, H. Ding, A. Döpp, J. Götzfried, S. Schindler, G. Schilling, S. Corde, A. Debus, T. Heinemann, B. Hidding, S. M. Hooker, A. Irman, O. Kononenko, T. Kurz, A. Martinez de la Ossa, U. Schramm, and S. Karsch, *Phys. Rev. X* **9**, 011046 (2019).
- [22] T. Kurz, T. Heinemann, M. F. Gilljohann, Y. Y. Chang, J. P. C. Cabadağ, A. Debus, O. Kononenko, R. Pausch, S. Schöbel, R. W. Assmann, M. Bussmann, H. Ding, J. Götzfried, A. Köhler, G. Raj, S. Schindler, K. Steiniger, O. Zarini, S. Corde, A. Döpp, B. Hidding, S. Karsch, U. Schramm, A. M. de la Ossa, and A. Irman, *Nature Communications* **12**, 2895 (2021).
- [23] J. P. Couperus Cabadağ, R. Pausch, S. Schöbel, M. Bussmann, Y.-Y. Chang, S. Corde, A. Debus, H. Ding, A. Döpp, F. M. Foerster, M. Gilljohann, F. Haberstroh, T. Heinemann, B. Hidding, S. Karsch, A. Koehler, O. Kononenko, A. Knetsch, T. Kurz, A. Martinez de la Ossa, A. Nutter, G. Raj, K. Steiniger, U. Schramm, P. Ufer, and A. Irman, *Phys. Rev. Research* **3**, L042005 (2021).
- [24] S. Schöbel, R. Pausch, Y.-Y. Chang, S. Corde, J. Couperus Cabadağ, A. Debus, H. Ding, A. Döpp, F. M. Foerster, M. Gilljohann, F. Haberstroh, T. Heinemann, B. Hidding, S. Karsch, A. Köhler, O. Kononenko, T. Kurz, A. Nutter, K. Steiniger, P. Ufer, A. Martinez de la Ossa, U. Schramm, and A. Irman, *New Journal of Physics* **24**, 083034 (2022).
- [25] A. R. Maier, N. M. Delbos, T. Eichner, L. Hübner, S. Jalas, L. Jeppe, S. W. Jolly, M. Kirchen, V. Leroux, P. Messner, M. Schnepf, M. Trunk, P. A. Walker, C. Werle, and P. Winkler, *Physical Review X* **10**, 031039 (2020).
- [26] D. Oumbarek Espinos, A. Rondepierre, A. Zhidkov, N. Pathak, Z. Jin, K. Huang, N. Nakanii, I. Daito, M. Kando, and T. Hosokai, *Scientific Reports* **13**, 18466 (2023).
- [27] A. Martinez de la Ossa, T. J. Mehrling, L. Schaper, M. J. V. Streeter, and J. Osterhoff, *Physics of Plasmas* **22**, 093107 (2015).
- [28] B. Hidding, G. Pretzler, J. B. Rosenzweig, T. Königstein, D. Schiller, and D. L. Bruhwiler, *Physical Review Letters* **108**, 035001 (2012).
- [29] S. N. A. Lab., *Technical Design Report for the FACET-II*

- Project at SLAC National Accelerator Laboratory*, Tech. Rep. (SLAC National Accelerator Lab., Menlo Park, CA (United States), 2016).
- [30] R. D’Arcy, A. Aschikhin, S. Bohlen, G. Boyle, T. Brümmer, J. Chappell, S. Diederichs, B. Foster, M. J. Garland, L. Goldberg, P. Gonzalez, S. Karstensen, A. Knetsch, P. Kuang, V. Libov, K. Ludwig, A. Martinez de la Ossa, F. Marutzky, M. Meisel, T. J. Mehrling, P. Niknejadi, K. Pöder, P. Pourmoussavi, M. Quast, J. H. Röckemann, L. Schaper, B. Schmidt, S. Schröder, J. P. Schwinkendorf, B. Sheeran, G. Tauscher, S. Wesch, M. Wing, P. Winkler, M. Zeng, and J. Osterhoff, *Philosophical Transactions of the Royal Society A: Mathematical, Physical and Engineering Sciences* **377**, 20180392 (2019).
- [31] E. Adli, A. Ahuja, O. Apsimon, R. Apsimon, A. M. Bachmann, D. Barrientos, F. Batsch, J. Bauche, V. K. B. Olsen, M. Bernardini, T. Bohl, C. Bracco, F. Braunmüller, G. Burt, B. Buttenschön, A. Caldwell, M. Cascella, J. Chappell, E. Chevallay, M. Chung, D. Cooke, H. Damerau, L. Deacon, L. H. Deubner, A. Dexter, S. Doebert, J. Farmer, V. N. Fedosseev, R. Fiorito, R. A. Fonseca, F. Friebel, L. Garolfi, S. Gessner, I. Gorgisyan, A. A. Gorn, E. Granados, O. Grulke, E. Gschwendtner, J. Hansen, A. Helm, J. R. Henderson, M. Hüther, M. Ibison, L. Jensen, S. Jolly, F. Keeble, S. Y. Kim, F. Kraus, Y. Li, S. Liu, N. Lopes, K. V. Lotov, L. M. Brun, M. Martyanov, S. Mazzoni, D. M. Godoy, V. A. Minakov, J. Mitchell, J. C. Molendijk, J. T. Moody, M. Moreira, P. Muggli, E. Oz, C. Pasquino, A. Pardons, F. P. Asmus, K. Pepitone, A. Perera, A. Petrenko, S. Pitman, A. Pukhov, S. Rey, K. Rieger, H. Ruhl, J. S. Schmidt, I. A. Shalimova, P. Sherwood, L. O. Silva, L. Soby, A. P. Sosedkin, R. Speroni, R. I. Spitsyn, P. V. Tuv, M. Turner, F. Velotti, L. Verra, V. A. Verzilov, J. Vieira, C. P. Welsch, B. Williamson, M. Wing, B. Woolley, and G. Xia (AWAKE), *Nature* **561**, 363 (2018).
- [32] R. Pompili, D. Alesini, M. P. Anania, M. Behtouei, M. Bellaveglia, A. Biagioni, F. G. Bisesto, M. Cesarini, E. Chiadroni, A. Cianchi, G. Costa, M. Croia, A. Del Dotto, D. Di Giovenale, M. Diomede, F. Dipace, M. Ferrario, A. Giribono, V. Lollo, L. Magnisi, M. Marongiu, A. Mostacci, L. Piersanti, G. Di Pirro, S. Romeo, A. R. Rossi, J. Scifo, V. Shpakov, C. Vaccarezza, F. Villa, and A. Zigler, *Nature Physics* **17**, 499–503 (2021).
- [33] See Supplemental Material at [URL will be inserted by publisher] for additional information on the experimental setup, parameters for simulations, and details on data analysis.
- [34] A. Martinez de la Ossa, R. W. Assmann, M. Bussmann, S. Corde, J. P. Couperus Cabadağ, A. Debus, A. Döpp, A. Ferran Pousa, M. F. Gilljohann, T. Heinemann, B. Hidding, A. Irman, S. Karsch, O. Kononenko, T. Kurz, J. Osterhoff, R. Pausch, S. Schöbel, and U. Schramm, *Philosophical Transactions of the Royal Society A: Mathematical, Physical and Engineering Sciences* **377**, 20180175 (2019).
- [35] B. Hidding, T. Königstein, J. Osterholz, S. Karsch, O. Willi, and G. Pretzler, *Physical Review Letters* **104**, 195002 (2010).
- [36] A. Irman, J. P. Couperus, A. Debus, A. Köhler, J. M. Krämer, R. Pausch, O. Zarini, and U. Schramm, *Plasma Physics and Controlled Fusion* **60**, 044015 (2018).
- [37] M. Mirzaie, S. Li, M. Zeng, N. A. M. Hafz, M. Chen, G. Y. Li, Q. J. Zhu, H. Liao, T. Sokollik, F. Liu, Y. Y. Ma, L. Chen, Z. M. Sheng, and J. Zhang, *Scientific Reports* **5**, 14659 (2015).
- [38] M. Zeng, M. Chen, Z.-M. Sheng, W. B. Mori, and J. Zhang, *Physics of Plasmas* **21**, 030701 (2014).
- [39] K. L. F. Bane, P. B. Wilson, and T. Weiland, in *AIP Conference Proceedings*, Vol. 127 (AIP, 1985) pp. 875–928.
- [40] C. Hue, A. Golovanov, S. Tata, S. Corde, and V. Malka, *Journal of Plasma Physics* **89**, 965890502 (2023).
- [41] C. Zhang, D. Storey, P. San Miguel Claveria, Z. Nie, K. A. Marsh, M. Hogan, W. B. Mori, E. Adli, W. An, R. Ariniello, G. J. Cao, C. Clarke, S. Corde, T. Dalichaouch, C. E. Doss, C. Emma, H. Ekerfelt, E. Gerstmayr, S. Gessner, C. Hansel, A. Knetsch, V. Lee, F. Li, M. Litos, B. O’Shea, G. White, G. Yocky, V. Zakharova, and C. Joshi, *Plasma Physics and Controlled Fusion* **66**, 025013 (2024).
- [42] F. Peña, C. A. Lindström, J. Beinortaitė, J. Björklund Svensson, L. Boulton, S. Diederichs, B. Foster, J. M. Garland, P. González Caminal, G. Loisch, S. Schröder, M. Thévenet, S. Wesch, J. C. Wood, J. Osterhoff, and R. D’Arcy, *Physical Review Research* **6**, 043090 (2024).
- [43] M. Litos, E. Adli, W. An, C. I. Clarke, C. E. Clayton, S. Corde, J. P. Delahaye, R. J. England, A. S. Fisher, J. Frederico, S. Gessner, S. Z. Green, M. J. Hogan, C. Joshi, W. Lu, K. A. Marsh, W. B. Mori, P. Muggli, N. Vafaei-Najafabadi, D. Walz, G. White, Z. Wu, V. Yakimenko, and G. Yocky, *Nature* **515**, 92 (2014).
- [44] C. A. Lindström, J. Beinortaitė, J. Björklund Svensson, L. Boulton, J. Chappell, S. Diederichs, B. Foster, J. M. Garland, P. González Caminal, G. Loisch, F. Peña, S. Schröder, M. Thévenet, S. Wesch, M. Wing, J. C. Wood, R. D’Arcy, and J. Osterhoff, *Nature Communications* **15**, 6097 (2024).
- [45] N. Vafaei-Najafabadi, W. An, C. E. Clayton, C. Joshi, K. A. Marsh, W. B. Mori, E. C. Welch, W. Lu, E. Adli, J. Allen, C. I. Clarke, S. Corde, J. Frederico, S. J. Gessner, S. Z. Green, M. J. Hogan, M. D. Litos, and V. Yakimenko, *Plasma Physics and Controlled Fusion* **58**, 034009 (2016).
- [46] A. Deng, O. S. Karger, T. Heinemann, A. Knetsch, P. Scherkl, G. G. Manahan, A. Beaton, D. Ullmann, G. Wittig, A. F. Habib, Y. Xi, M. D. Litos, B. D. O’Shea, S. Gessner, C. I. Clarke, S. Z. Green, C. A. Lindström, E. Adli, R. Zgadzaj, M. C. Downer, G. Andonian, A. Murokh, D. L. Bruhwiler, J. R. Cary, M. J. Hogan, V. Yakimenko, J. B. Rosenzweig, and B. Hidding, *Nature Physics* **15**, 1156 (2019).
- [47] A. Knetsch, B. Sheeran, L. Boulton, P. Niknejadi, K. Pöder, L. Schaper, M. Zeng, S. Bohlen, G. Boyle, T. Brümmer, J. Chappell, R. D’Arcy, S. Diederichs, B. Foster, M. J. Garland, P. Gonzalez Caminal, B. Hidding, V. Libov, C. A. Lindström, A. Martinez de la Ossa, M. Meisel, T. Parikh, B. Schmidt, S. Schröder, G. Tauscher, S. Wesch, P. Winkler, J. C. Wood, and J. Osterhoff, *Phys. Rev. Accel. Beams* **24**, 101302 (2021).
- [48] D. Ullmann, P. Scherkl, A. Knetsch, T. Heinemann, A. Sutherland, A. F. Habib, O. S. Karger, A. Beaton, G. G. Manahan, A. Deng, G. Andonian, M. D. Litos, B. D. O’Shea, J. R. Cary, M. J. Hogan, V. Yakimenko,

- J. B. Rosenzweig, and B. Hidding, *Phys. Rev. Research* **3**, 043163 (2021).
- [49] P. Chen, J. J. Su, J. M. Dawson, K. L. F. Bane, and P. B. Wilson, *Physical Review Letters* **56**, 1252 (1986).
- [50] K. V. Lotov, *Physics of Plasmas* **12**, 053105 (2005).
- [51] Q. Su, J. Larson, T. N. Dalichaouch, F. Li, W. An, L. Hildebrand, Y. Zhao, V. Decyk, P. Alves, S. M. Wild, and W. B. Mori, *Physics of Plasmas* **30**, 053108 (2023).
- [52] G. Loisch, G. Asova, P. Boonpornprasert, R. Brinkmann, Y. Chen, J. Engel, J. Good, M. Gross, F. Grüner, H. Huck, D. Kalantaryan, M. Krasilnikov, O. Lishilin, A. M. de la Ossa, T. J. Mehrling, D. Melkumyan, A. Oepelt, J. Osterhoff, H. Qian, Y. Renier, F. Stephan, C. Tenholt, V. Wohlfarth, and Q. Zhao, *Physical Review Letters* **121**, 064801 (2018).
- [53] R. Roussel, G. Andonian, W. Lynn, K. Sanwalka, R. Robles, C. Hansel, A. Deng, G. Lawler, J. B. Rosenzweig, G. Ha, J. Seok, J. G. Power, M. Conde, E. Wisniewski, D. S. Doran, and C. E. Whiteford, *Physical Review Letters* **124**, 044802 (2020).
- [54] M. Labat, J. C. Cabadağ, A. Ghaith, A. Irman, A. Berlioux, P. Berteaud, F. Blache, S. Bock, F. Bouvet, F. Briquez, Y.-Y. Chang, S. Corde, A. Debus, C. De Oliveira, J.-P. Duval, Y. Dietrich, M. El Ajjouri, C. Eisenmann, J. Gautier, R. Gebhardt, S. Grams, U. Helbig, C. Herbeaux, N. Hubert, C. Kitegi, O. Kononenko, M. Kuntzsch, M. LaBerge, S. Lê, B. Leluan, A. Loulergue, V. Malka, F. Marteau, M. H. N. Guyen, D. Oumbarek-Espinos, R. Pausch, D. Pereira, T. Püschel, J.-P. Ricaud, P. Rommeluere, E. Roussel, P. Rousseau, S. Schöbel, M. Sebdaoui, K. Steiniger, K. Tavakoli, C. Thauray, P. Ufer, M. Valléau, M. Vandenberghe, J. Vétéran, U. Schramm, and M.-E. Couprie, *Nature Photonics* **17**, 150–156 (2022).
- [55] W. Wang, K. Feng, L. Ke, C. Yu, Y. Xu, R. Qi, Y. Chen, Z. Qin, Z. Zhang, M. Fang, J. Liu, K. Jiang, H. Wang, C. Wang, X. Yang, F. Wu, Y. Leng, J. Liu, R. Li, and Z. Xu, *Nature* **595**, 516 (2021).
- [56] S. K. Barber, F. Kohrell, C. E. Doss, K. Jensen, C. Berger, F. Isono, Z. Eisentraut, S. Schröder, A. J. Gonsalves, K. Nakamura, G. R. Plateau, R. A. van Mourik, M. Gracia-Linares, L. Labun, B. M. Hegelich, S. V. Milton, C. G. R. Geddes, J. Osterhoff, C. B. Schroeder, E. H. Esarey, and J. van Tilborg, *Physical Review Letters* **135**, 055001 (2025).
- [57] F. Habib, P. Scherkl, G. G. Manahan, T. Heinemann, D. Ullmann, A. Sutherland, A. Knetsch, M. Litos, M. Hogan, J. Rosenzweig, and B. Hidding, in *Advances in Laboratory-based X-Ray Sources, Optics, and Applications VII*, edited by A. Murokh and D. Spiga (SPIE, San Diego, United States, 2019) p. 9.
- [58] A. F. Habib, G. G. Manahan, P. Scherkl, T. Heinemann, A. Sutherland, R. Altuiri, B. M. Alotaibi, M. Litos, J. Cary, T. Raubenheimer, E. Hemsing, M. J. Hogan, J. B. Rosenzweig, P. H. Williams, B. W. J. McNeil, and B. Hidding, *Nature Communications* **14**, 1054 (2023).
- [59] R. Weingartner, S. Raith, A. Popp, S. Chou, J. Wenz, K. Khrennikov, M. Heigoldt, A. Maier, N. Kajumba, M. Fuchs, B. Zeitler, F. Krausz, S. Karsch, and F. Gruner, *Physical Review Special Topics-Accelerators and Beams* **15**, 111302 (2012).
- [60] F. C. Salgado, K. Grafenstein, A. Golub, A. Döpp, A. Eckey, D. Hollatz, C. Müller, A. Seidel, D. Seipt, S. Karsch, and M. Zepf, *New Journal of Physics* **23**, 105002 (2021).
- [61] E. Adli, J. Appleby, T. L. Barklow, M. Biagini, J. B. Svensson, M. Berggren, S. Bettoni, S. Boogert, P. Burrows, A. Caldwell, J. B. B. Chen, V. Cilento, L. Corner, R. D’Arcy, S. Doebert, W. Dou, P. Drobnik, C. Dyson, S. Farrington, J. Farmer, A. Faus-Golfe, M. Formela, A. Formenti, L. Forrester, B. Foster, J. Gao, S. Gessner, N. Hamann, A. Harrison, M. J. Hogan, E. E. Hørlyk, D. Kalvik, A. Laudrain, R. Lehe, W. Leemans, C. A. Lindstrøm, B. List, J. List, X. Lu, E. Mactavish, V. Maslov, E. Nanni, J. Osborne, J. Osterhoff, F. Peña, G. M. Pick, K. Pöder, J. Reuter, D. Samoilenko, N. Sedlackova, A. Seryi, K. Sjobak, T. Sloan, S. Stapnes, R. T. Garcia, M. Titov, M. Trautwein, M. Thévenet, N. J. Walker, M. Wenskat, M. Wing, and J. Wood, *HALHF: A hybrid, asymmetric, linear Higgs factory using plasma- and RF-based acceleration* (2025).

Supplemental Material: Efficient Acceleration of High-Quality GeV-Electron Bunches in a Hybrid Laser- and Beam-Driven Plasma Wakefield Accelerator

F. M. Foerster,^{1,*} M. Ayache,¹ Z. Bi,¹ M. Cerchez,² S. Corde,³ A. Döpp,^{1,4}
F. Haberstroh,¹ A. F. Habib,⁵ T. Heinemann,² B. Hidding,² A. Irman,⁶ F.
Irshad,¹ O. Kononenko,³ M. LaBerge,⁶ A. Martinez de la Ossa,⁷ A. Münzer,¹
F. Peña,^{1,8} G. Schilling,¹ S. Schöbel,^{6,9} U. Schramm,^{6,9} S. Sharan,¹ E.
Travac,¹ P. Ufer,^{6,9} N. Weiße,¹ M. Zeuner,¹ J. Zirkelbach,¹ and S. Karsch^{1,4,†}

¹*Ludwig-Maximilians-Universität München,
Am Coulombwall 1, 85748 Garching, Germany*

²*Heinrich Heine Universität Düsseldorf,
Universitätsstraße 1, 40225 Düsseldorf, Germany*

³*Laboratoire d'Optique Appliquée (LOA),
CNRS, École polytechnique, ENSTA,
Institut Polytechnique de Paris, Palaiseau, France*

⁴*Max Planck Institut für Quantenoptik,
Hans-Kopfermann-Strasse 1, 85748 Garching, Germany*

⁵*University of Strathclyde, 107 Rottenrow,
Glasgow G4 0NG, United Kingdom*

⁶*Helmholtz-Zentrum Dresden-Rossendorf,
Bautzner Landstrasse 400, 01328 Dresden, Germany*

⁷*Deutsches Elektronen-Synchrotron DESY,
Notkestraße 85, 22607 Hamburg, Germany*

⁸*Department of Physics, University of Oslo, 0316, Oslo, Norway*

⁹*Technische Universität Dresden, 01062 Dresden, Germany*

(Dated: March 2, 2026)

ANALYSIS OF DRIVER-TO-WITNESS EFFICIENCY

To quantify the energy transfer efficiency from driver to witness we use the following definition in our analysis:

$$\eta_{D \rightarrow W} = \frac{\Delta \varepsilon_W}{\varepsilon_D}.$$

The calculated efficiency values are subject to different types of uncertainties. The integrated energy of driver and witness $\varepsilon_{D/W} = \int \rho_Q(E) E dE$ fluctuates due to shot-to-shot variations of the spectral charge density ρ_Q , i.e. of bunch charge and peak energy of both bunches. Examining set averages, these shot-to-shot variations are by far the largest contributors to the uncertainty interval. For the drive bunches, the relative standard deviation of the integrated energy is approximately 20%. For the witness bunch, the value of these fluctuations depends on the injection position. For the highest-energy witness bunches, those injected at the very front of the PWFA target, the shot-to-shot fluctuations peak at a relative standard deviation of approximately 70%.

Furthermore, individual shots are subject to measurement uncertainties, which, however, are significantly lower than the shot-to-shot fluctuations:

The absolute charge calibration of our dipole spectrometer does not pose a major problem, as the charge calibration constant cancels out by dividing the integrated energies of both bunches.

The energy calibration of the spectrometer is an issue. In particular, the measured energy depends on the pointing of the electron beams due to the trajectory of the electron beams in the dipole spectrometer. No pointing screen was used for the data presented in this article, as this increases beam divergence; thus, beam quality and energy cannot be measured accurately simultaneously.

Instead, we estimate the energy uncertainty by analyzing the pointing jitter in a different run under similar conditions. We measure shot-to-shot pointing fluctuations of 5 mrad (standard deviation), which corresponds to an energy error of $\pm 5\%$ for our dipole spectrometer at a peak energy of 1 GeV. Furthermore, we don't observe any significant correlation between pointing and peak energy of the witness, i.e. the shot-to-shot fluctuations in energy are larger than the effect of varying pointing.

A general problem with PWFA experiments is that we cannot measure drive bunch

properties before and after the PWFA stage individually on a single shot.

To account for the sum of these effects, we estimate a lower limit for the peak driver-to-witness energy transfer efficiency by dividing the integrated witness energy of the best single shot by the highest integrated driver energy measured among all analyzed LWFA shots.

COMPARISON OF PWFA RESULTS

In Table I, we present an overview of driver and witness parameters, transformer ratio, and energy transfer efficiencies reported from PWFA experiments. The data from this table have been used to compile Figure 4 of the manuscript. We would like to point out that not all authors provide exactly identical definitions of the beam parameters cited here. Some of the values were taken only approximately from the authors' figures. However, this does not fundamentally affect their comparability. The values for blank spaces in the table could not be determined from or do not apply to the respective publications.

PARTICLE IN CELL SIMULATIONS

This paragraph provides information on the input of the PIC simulations of the PWFA stage used in Figure 1 of the manuscript. The physical parameters are similar to our experiments and the results reproduce our experiment qualitatively.

We use the PIC-code FBPIC (Fourier-Bessel Particle-In-Cell) [19, 20]. We make use of the cylindrical coordinate system used in FBPIC, by assuming complete rotational symmetry and, therefore, use only one azimuthal mode. To resolve the injection of the witness bunch at the density transition, we use a spatial resolution of $\Delta z = 100$ nm and $\Delta r = 350$ nm. Furthermore, we increase the number of macroparticles per cell around the density transition to $n_z = 10$ (Number of particles per cell along z), $n_r = 4$ (along r), and $n_t = 1$ (along theta), while it is 2, 2, and 1, respectively, elsewhere.

The plasma density profile is presented in Figure 1 of the manuscript and models the one we retrieved from interferometry of the plasma.

We initialize the phase space of the drive bunch, approximating the experimental measurements. The driver's mean energy is 700 MeV, with an uncorrelated energy spread of 10 MeV (rms), and a linear chirp leading to a correlated energy spread of 200 MeV. The

TABLE I. Overview of beam parameters, transformer ratio, and energy transfer efficiencies reported from PWFA experiments. Witness and driver charges are denoted by Q_W and Q_D . ΔE_W is the witness energy gain and E_D the initial driver energy. $\frac{\delta E_W}{E_W}$ is the relative energy spread of the witness bunch. $\eta_{D \rightarrow W}$ is the overall driver-to-witness energy transfer efficiency, and $\eta_{P \rightarrow W}$ is the plasma-to-witness energy transfer efficiency.

Publication	Driver	Q_D	E_D	Inj.	Q_W	ΔE_W	$\frac{\delta E_W}{E_W}$	$\eta_{D \rightarrow W}$	$\eta_{P \rightarrow W}$	$\frac{\Delta E_W}{E_D}$
		[pC]	[MeV]		[pC]	[MeV]	[%]	[%]	[%]	[%]
This work, Fig. 2(c)	LWFA	366	716	int.	48	930	4.1 (FWHM)	≥ 9.5	≥ 21	130
This work, Fig. 2(d)	LWFA	366	716	int.	53	1080	6.9 (FWHM)	≥ 17	≥ 39	150
This work, Fig. 2(e)	LWFA	366	716	int.	38	1280	3.1 (FWHM)	≥ 7.0	≥ 16	180
Blumenfeld2007 [1]	rf		42000	ext.		44000				105
Litos2014 [2]	rf	1020	20350	ext.	74	1600	2 (rms)	0.6	29	8
Litos2016 [3]	rf	600	20350	ext.	120	5300	5 (rms)	5.2		26
Vafaei-Najafabadi2016 [4]	rf	2880	20350	int.	25	30000	20 (FWHM)	1.3		150
Loisch2018 [5]	rf	500	25	ext.	3	0.4		0.01		1.6
Deng2019 [6]	rf	3200	20350	int.	100	500	2.5 (rms)	0.1		2.5
Roussel2020 [7]	rf	1600	40	ext.		1				2.5
Lindstrom2021 [8]	rf	500	1000	ext.	100	45	0.13 (FWHM)	0.9	42	5
Knetsch2021 [9]	rf	790	1116	int.	33	45	4.4 (rms)	0.2		4
Ullmann2021 [10]	rf	3200	20000	int.	500	780	6.4 (rms)	0.6		4
Kurz2021 [11]	LWFA	104	260	ext.	12	66	6 (FWHM)	2.9		25
Pompili2021 [12]	rf	350	89.5	ext.	20	6.8	0.1 (rms)	0.4		8
Foerster2022 [13]	LWFA	650	250	int.	30	162	3.5 (FWHM)	3		65
Lindstrom2024 [14]	rf	400	1050	ext.	40	40	0.09 (FWHM)	0.4	22	4
Wood2024 [15]	rf	230	1200	ext.	40	250	0.17 (FWHM)	3.6		21
Zhang2024 [16]	rf	1600	10000	ext.		8000				80
Zhang2025 [17]	rf	1600	10000	int.	2.3	26000	0.7 (rms)	0.4		260
Wood2026 [18]	rf	304	689	int.	19	30	1.3 (FWHM)	0.3		4.4

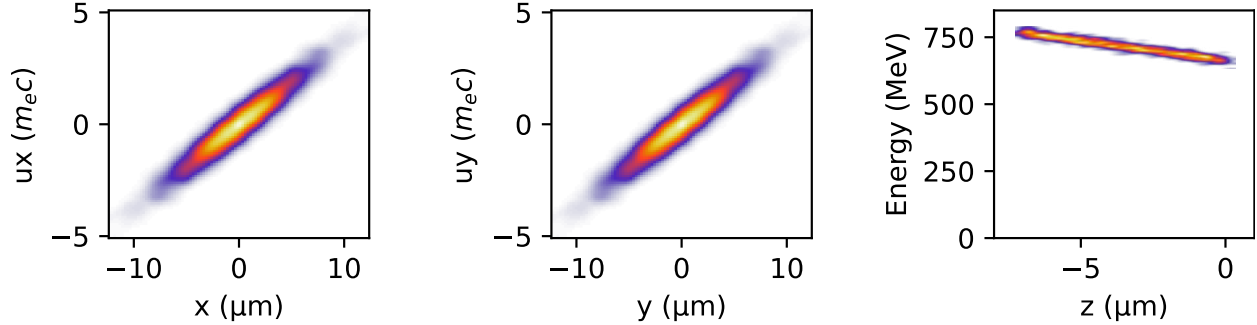


FIG. 1. Transverse and longitudinal phase space distributions of the simulated drive bunch just before entering the PWFA stage.

bunch length is $7\ \mu\text{m}$. Source size and divergence of the driver are set to $1\ \mu\text{m}$ (rms) and $1\ \text{mrad}$ (rms), respectively. The phase space of the drive bunch just before entering the PWFA target is shown in Figure 1.

* moritz.foerster@physik.uni-muenchen.de

† stefan.karsch@physik.uni-muenchen.de

- [1] I. Blumenfeld, C. E. Clayton, F. J. Decker, M. J. Hogan, C. K. Huang, R. Ischebeck, R. Iverson, C. Joshi, T. Katsouleas, N. Kirby, W. Lu, K. A. Marsh, W. B. Mori, P. Muggli, E. Oz, R. H. Siemann, D. Walz, and M. M. Zhou, *Nature* **445**, 741 (2007).
- [2] M. Litos, E. Adli, W. An, C. I. Clarke, C. E. Clayton, S. Corde, J. P. Delahaye, R. J. England, A. S. Fisher, J. Frederico, S. Gessner, S. Z. Green, M. J. Hogan, C. Joshi, W. Lu, K. A. Marsh, W. B. Mori, P. Muggli, N. Vafaei-Najafabadi, D. Walz, G. White, Z. Wu, V. Yakimenko, and G. Yocky, *Nature* **515**, 92 (2014).
- [3] M. Litos, E. Adli, J. M. Allen, W. An, C. I. Clarke, S. Corde, C. E. Clayton, J. Frederico, S. J. Gessner, S. Z. Green, M. J. Hogan, C. Joshi, W. Lu, K. A. Marsh, W. B. Mori, M. Schmeltz, N. Vafaei-Najafabadi, and V. Yakimenko, *Plasma Physics and Controlled Fusion* **58**, 034017 (2016).
- [4] N. Vafaei-Najafabadi, W. An, C. E. Clayton, C. Joshi, K. A. Marsh, W. B. Mori, E. C. Welch, W. Lu, E. Adli, J. Allen, C. I. Clarke, S. Corde, J. Frederico, S. J. Gessner, S. Z. Green, M. J. Hogan, M. D. Litos, and V. Yakimenko, *Plasma Physics and Controlled Fusion* **58**, 034009 (2016).

- [5] G. Loisch, G. Asova, P. Boonpornprasert, R. Brinkmann, Y. Chen, J. Engel, J. Good, M. Gross, F. Grüner, H. Huck, D. Kalantaryan, M. Krasilnikov, O. Lishilin, A. M. de la Ossa, T. J. Mehrling, D. Melkumyan, A. Oppelt, J. Osterhoff, H. Qian, Y. Renier, F. Stephan, C. Tenholt, V. Wohlfarth, and Q. Zhao, *Physical Review Letters* **121**, 064801 (2018).
- [6] A. Deng, O. S. Karger, T. Heinemann, A. Knetsch, P. Scherkl, G. G. Manahan, A. Beaton, D. Ullmann, G. Wittig, A. F. Habib, Y. Xi, M. D. Litos, B. D. O’Shea, S. Gessner, C. I. Clarke, S. Z. Green, C. A. Lindstrøm, E. Adli, R. Zgadzaj, M. C. Downer, G. Andonian, A. Murokh, D. L. Bruhwiler, J. R. Cary, M. J. Hogan, V. Yakimenko, J. B. Rosenzweig, and B. Hidding, *Nature Physics* **15**, 1156 (2019).
- [7] R. Roussel, G. Andonian, W. Lynn, K. Sanwalka, R. Robles, C. Hansel, A. Deng, G. Lawler, J. B. Rosenzweig, G. Ha, J. Seok, J. G. Power, M. Conde, E. Wisniewski, D. S. Doran, and C. E. Whiteford, *Physical Review Letters* **124**, 044802 (2020).
- [8] C. A. Lindstrøm, J. M. Garland, S. Schröder, L. Boulton, G. Boyle, J. Chappell, R. D’Arcy, P. Gonzalez, A. Knetsch, V. Libov, G. Loisch, A. Martinez de la Ossa, P. Niknejadi, K. Pöder, L. Schaper, B. Schmidt, B. Sheeran, S. Wesch, J. Wood, and J. Osterhoff, *Phys. Rev. Lett.* **126**, 014801 (2021).
- [9] A. Knetsch, B. Sheeran, L. Boulton, P. Niknejadi, K. Pöder, L. Schaper, M. Zeng, S. Bohlen, G. Boyle, T. Brümmer, J. Chappell, R. D’Arcy, S. Diederichs, B. Foster, M. J. Garland, P. Gonzalez Caminal, B. Hidding, V. Libov, C. A. Lindstrøm, A. Martinez de la Ossa, M. Meisel, T. Parikh, B. Schmidt, S. Schröder, G. Tauscher, S. Wesch, P. Winkler, J. C. Wood, and J. Osterhoff, *Phys. Rev. Accel. Beams* **24**, 101302 (2021).
- [10] D. Ullmann, P. Scherkl, A. Knetsch, T. Heinemann, A. Sutherland, A. F. Habib, O. S. Karger, A. Beaton, G. G. Manahan, A. Deng, G. Andonian, M. D. Litos, B. D. OShea, J. R. Cary, M. J. Hogan, V. Yakimenko, J. B. Rosenzweig, and B. Hidding, *Phys. Rev. Research* **3**, 043163 (2021).
- [11] T. Kurz, T. Heinemann, M. F. Gilljohann, Y. Y. Chang, J. P. C. Cabadağ, A. Debus, O. Kononenko, R. Pausch, S. Schöbel, R. W. Assmann, M. Bussmann, H. Ding, J. Götzfried, A. Köhler, G. Raj, S. Schindler, K. Steiniger, O. Zarini, S. Corde, A. Döpp, B. Hidding, S. Karsch, U. Schramm, A. M. de la Ossa, and A. Irman, *Nature Communications* **12**, 2895 (2021).
- [12] R. Pompili, D. Alesini, M. P. Anania, M. Behtouei, M. Bellaveglia, A. Biagioni, F. G. Bisesto,

- M. Cesarini, E. Chiadroni, A. Cianchi, G. Costa, M. Croia, A. Del Dotto, D. Di Giovenale, M. Diomede, F. Dipace, M. Ferrario, A. Giribono, V. Lollo, L. Magnisi, M. Marongiu, A. Mostacci, L. Piersanti, G. Di Pirro, S. Romeo, A. R. Rossi, J. Scifo, V. Shpakov, C. Vaccarezza, F. Villa, and A. Zigler, *Nature Physics* **17**, 499–503 (2021).
- [13] F. M. Foerster, A. Döpp, F. Haberstroh, K. v. Grafenstein, D. Campbell, Y.-Y. Chang, S. Corde, J. P. Couperus Cabadağ, A. Debus, M. F. Gilljohann, A. F. Habib, T. Heinemann, B. Hidding, A. Irman, F. Irshad, A. Knetsch, O. Kononenko, A. Martinez de la Ossa, A. Nutter, R. Pausch, G. Schilling, A. Schletter, S. Schöbel, U. Schramm, E. Travac, P. Ufer, and S. Karsch, *Physical Review X* **12**, 041016 (2022).
- [14] C. A. Lindstrøm, J. Beinortaitė, J. Björklund Svensson, L. Boulton, J. Chappell, S. Diederichs, B. Foster, J. M. Garland, P. González Caminal, G. Loisch, F. Peña, S. Schröder, M. Thévenet, S. Wesch, M. Wing, J. C. Wood, R. D’Arcy, and J. Osterhoff, *Nature Communications* **15**, 6097 (2024).
- [15] J. W. et al., in *Proc. IPAC’24*, IPAC’24 - 15th International Particle Accelerator Conference No. 15 (JACoW Publishing, Geneva, Switzerland, 2024) pp. 541–544.
- [16] C. Zhang, D. Storey, P. San Miguel Claveria, Z. Nie, K. A. Marsh, M. Hogan, W. B. Mori, E. Adli, W. An, R. Ariniello, G. J. Cao, C. Clarke, S. Corde, T. Dalichaouch, C. E. Doss, C. Emma, H. Ekerfelt, E. Gerstmayr, S. Gessner, C. Hansel, A. Knetsch, V. Lee, F. Li, M. Litos, B. O’Shea, G. White, G. Yocky, V. Zakharova, and C. Joshi, *Plasma Physics and Controlled Fusion* **66**, 025013 (2024).
- [17] C. Zhang, D. Storey, A. Knetsch, B. D. O’Shea, R. Ariniello, G. J. Cao, S. Corde, T. N. Dalichaouch, C. Emma, O. G. Finnerud, S. Gessner, C. Hansel, E. Hansen, V. Lee, C. A. Lindstrøm, M. Litos, N. Majernik, K. A. Marsh, W. B. Mori, I. Rajkovic, M. J. Hogan, and C. Joshi, *Nature Communications* **16**, 10719 (2025).
- [18] J. C. Wood, L. Boulton, J. Beinortaitė, J. Björklund Svensson, S. Bohlen, G. Boyle, J. M. Garland, P. Gonzalez Caminal, C. A. Lindstrøm, G. Loisch, S. M. Mewes, T. Parikh, F. Peña, K. Pöder, S. Schröder, M. Thévenet, S. Wesch, J. Osterhoff, and R. D’Arcy, *Nature Communications* **17**, 1588 (2026).
- [19] Fbpic documentation, <https://fbpic.github.io> (2016), accessed: 2023-07-30.
- [20] R. Lehe, M. Kirchen, I. A. Andriyash, B. B. Godfrey, and J.-L. Vay, *Computer Physics Communications* **203**, 66 (2016).